Spontaneous formation of one-dimensional ripples in transit to highly ordered two-dimensional herringbone structures through sequential and unequal biaxial mechanical stretching

Pei-Chun Lin and Shu Yang[a)]
Department of Materials Science and Engineering, University of Pennsylvania, 3231 Walnut Street, Philadelphia, Pennsylvania 19104

(Received 10 April 2007; accepted 7 May 2007; published online 12 June 2007)

The authors report the formation of various submicron wrinkle patterns and their transition from one-dimensional (1D) ripples to two-dimensional (2D) herringbone structures on poly(dimethylsiloxane) films. Using mechanical force they can separately control the amount and timing of strain applied to the substrate on both planar directions (either simultaneously or sequentially), which appears to be critical to maneuver the pattern formation in real time. They demonstrate reversible transitions from flat to 1D ripple, to ripple with bifurcation, to ripple/herringbone mixed features, and to well-controlled formation of a highly ordered zigzag-based 2D herringbone structures. © *2007 American Institute of Physics*. [DOI: 10.1063/1.2743939]

The ability to actively induce features and textures on surfaces has been of great interest for many potential applications, including stretchable electronics, microlens arrays, microelectromechanical systems, tunable surface adhesion and friction, and robotics.[1–4] One widely adopted simple and effective approach is based on the internal buckling force equilibrium within materials by coating a hard thin layer[5,6] on top of a prestrained bulk substrate, such as poly(dimethylsiloxane) (PDMS), followed by release of the pre-strain. During release, the self-organized wrinkles are formed simultaneously and permanently without further continuous input of external force or energy. Theoretical calculation has suggested that it is possible to form various wrinkle patterns by adjusting relative strain level between planar directions.[7,8] However, few have shown dynamic tuning between one-dimensional (1D) ripples and two-dimensional (2D) herringbone structures nor understanding of the transition mechanism experimentally.

While most wrinkle structures are formed by heat-induced-strain method, here we report the wrinkle formation induced by mechanical force on an oxidized PDMS film which allows us to independently control the amount and timing of strain applied on both planar directions (either simultaneously or sequentially). This added controllability appears critical to maneuver the pattern formation and transition *in real time*.

PDMS precursor (RTV615 from GE Silicones) was mixed with curing agent (10:1) and cured at 65 °C for 4 h. Then a square-shaped PDMS strip ($30\times30\times0.5$ mm^3) was clamped [Fig. 1(a)] and stretched 20% [25→30 mm, Fig. 1(b)] in both planar directions sequentially (*Y* first then *X*). The stretched sample was then treated with oxygen plasma [Fig. 1(c), Technics, model PE11-A], followed by release in the reverse order (*X* first then *Y*) to prevent sample warping and generate wrinkle patterns uniformly [Fig. 1(d)]. We observed a highly ordered zigzag-based herringbone pattern. As shown in the scanning electron microscopy (SEM) and atomic force microscopy (AFM) images [Fig. 1(e)], the edges of zigzags are parallel to each other and geometrical parameters (lengths, widths and height) of zigzags are uniform with very small deviations. In contrast, when another set of samples were stretched/released simultaneously in both planar directions with equal strain level, a much disordered zigzag-based herringbone pattern was observed [Fig. 1(f)], which was typical in heat-induced-strain wrinkle patterns.[9] In the latter case, the strains are applied and released simultaneously with equal strain level, thus, competing for energy minimization in all three spatial directions.

We performed a series of *in situ* study to investigate the pattern formation and transition during sequential and equal stretch/release [Figs. 2(a)–2(j)]. We kept the same stretch conditions of the sample (*Y* first and *X* second). After oxygen plasma before releasing, no pattern was formatted [Fig. 2(a)]. During the first release process in the *X* direction [Figs. 2(a)–2(e)] while keeping *Y* unchanged [Fig. 2(k)], we observed a periodic ripple pattern formed immediately once the stress in the sample passed the critical stress for buckling [Fig. 2(b)]. It agreed with the qualitative estimation using simplified buckling theories[7,10] and experimental observation by others.[2,6] The ripple width decreased gradually during release [Figs. 2(c) and 2(d)] until the sample was completely

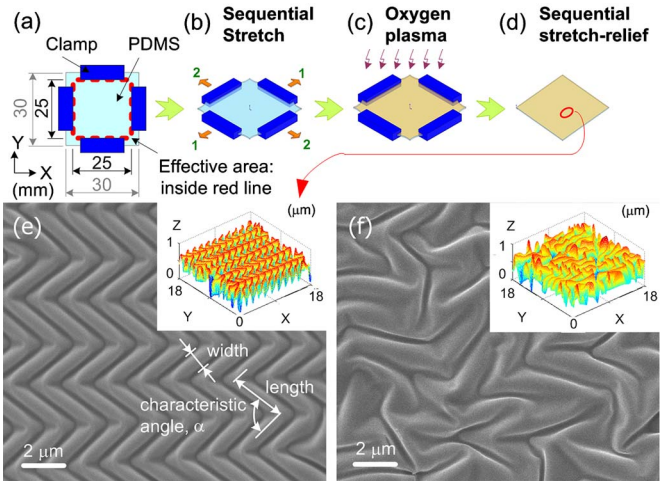

FIG. 1. (Color online) Schematic fabrication process to generate wrinkle patterns [(a)–(d)]. SEM and AFM images of surface patterns when stretching/release of PDMS film either sequentially [(e)] or simultaneously [(f)].

[a)]Electronic mail: shuyang@seas.upenn.edu

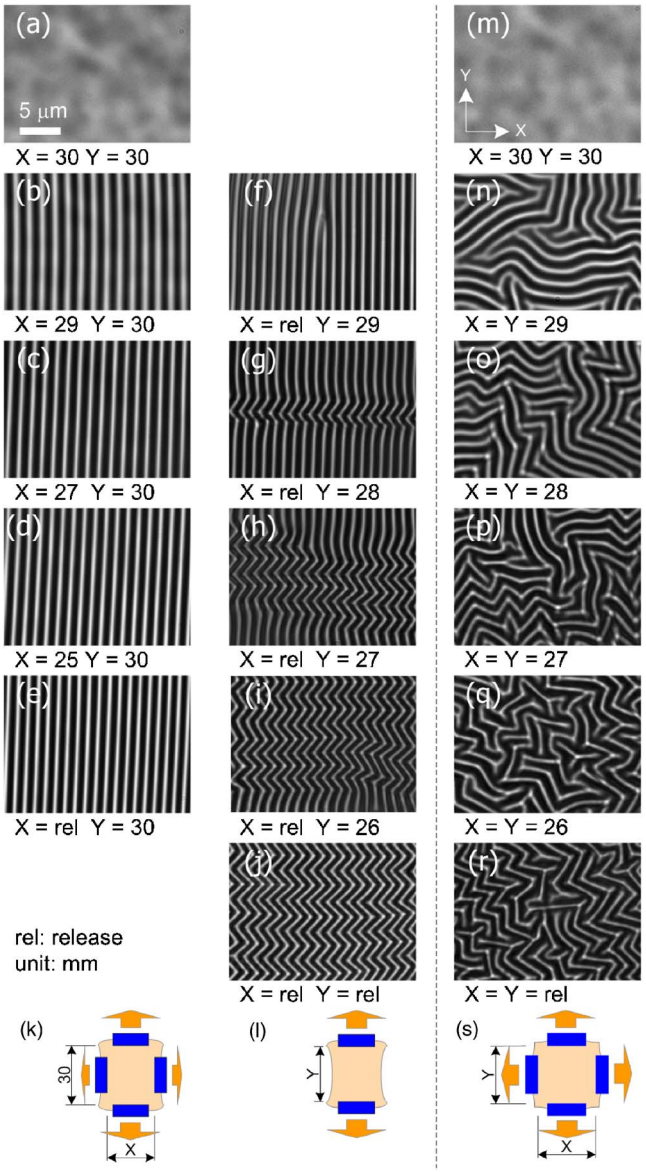

FIG. 2. (Color online) Two sets of sequential optical microscope images of two equal-stretched PDMS samples (20% strain) subjected to two different stretch releasing processes: sequentially [(a)–(j)] and simultaneously [(m)–(r)], respectively, and their corresponding illustrative sketches, (k)–(l) and (s), respectively. Scale bar in (a) is applicable to all images.

restored in the *X* direction [Fig. 2(e)]. When we started to release the stretch in the *Y* direction as well [Fig. 2(l)], ripple bifurcation was observed and found dispersed randomly and irregularly throughout the sample [Fig. 2(f)], which could be attributed to initiation of interfacial strain in the second planar direction. When the release proceeded further, the zigzag bending started to occur on the original ripple pattern [Fig. 2(g)] and increased [Figs. 2(h) and 2(i)]. When the stretch was fully released, the 1D ripple columns were bent completely into zigzag shape, forming the highly ordered herringbone structure [Fig. 2(j)] as the lowest energy state.[11] The wrinkle patterns formed during *in situ* release agree well with the observed final structures, as shown in Figs. 1(e). The same *in situ* studies were performed to simultaneously stretch/release PDMS films in both the *X* and *Y* directions [Figs. 2(m)–2(r)] resulting in immediate formation of irregular herringbone pattern [Fig. 2(n)]. The width of herringbone continued to decrease with the increase of the wrinkle density [Figs. 2(o)–2(q)] until the prestrain was completely relieved in both directions [Fig. 2(r)].

The above study implies that the key to generate highly ordered zigzag-based herringbone pattern lies in the strategy of sequential stretch/release, specifically the release part. For a sample that is stretched sequentially and equally, the first release in the *X* direction generates highly ordered 1D ripple patterns. When the stretch is released in the second *Y* direction, the sample surface subjected to this *Y*-direction buckling force is no longer a 2D flat plane but an array of ripple-shaped columns. The width of ripple remained unchanged during the second release [Figs. 2(f)–2(j)] confirms this concept. It is worth noting that the formation mechanism is in principle different from buckling a flat 2D surface in biaxial directions simultaneously. Because of this intrinsic difference, we observed obvious wavelength difference shown in Figs. 2(e) and 2(f). This orientation-regulating mechanism in sequential release by generating ripple structure first guarantees the alignment of zigzag pattern directions after the second release. The sequential release strategy indeed provides a well-controlled energy release path for the formation of highly ordered zigzag-based herringbone pattern which is proven to have a minimum elastic energy.[7,8] Another advantage of the mechanoinduced wrinkle patterns is that we can dynamically and reversibly tune the surface topography in real time from flat, to ripple, gradually to herringbone, and vice versa by varying the strain amount applied to the sample.

In both sequential release in the first *X* direction [Figs. 2(a)–2(e)] and simultaneous release [Figs. 2(m)–2(r)] cases, we observed that the wrinkle pattern formed immediately on the originally flat surface once the compression spring force of substrate passed the critical buckling force. Further release did not change the shape of pattern, and most of the released strain deformation contributed directly to the increase of wrinkle amplitude as predicted by recent nonlinear theories.[7,8] For the release in the second *Y* direction in the sequential release case, it had been thought that the strain should not contribute to generate extra amplitudes on the ripples but to release in side directions where the ripple was bent into zigzag patterns with a characteristic angle α defined in Fig. 1(e). However, instead of forming zigzags all over the ripple columns with α gradually increased from 0° to 90° during release, zigzag herringbones with $\alpha \sim 80° - 100°$ were formed on arbitrary locations immediately and propagating across the whole ripple columns as the release proceeded. We believe that zigzags should be initiated at the weakest section of the column. Similar explanation could be applied to the formation of ripple bifurcation.

Since formation of the herringbone pattern should be attributed to gradual buckling of the ripple column during the second release process there should exist certain geometric and characteristic relation between this intermediate-stage ripple (still with strain in one direction due to stretch) and final herringbone patterns. One widely adopted 1D analysis shows that initial buckling geometry, which is based on partially linear partially nonlinear stability analysis of a thin high-modulus layer on a semi-infinite low-modulus substrate,[2,7,8] can be described as

$$\lambda_0 = \frac{\pi t}{\sqrt{\varepsilon_c}} A_0 = t\sqrt{\frac{\varepsilon_{\mathrm{pre}}}{\varepsilon_c} - 1}, \tag{1}$$

where

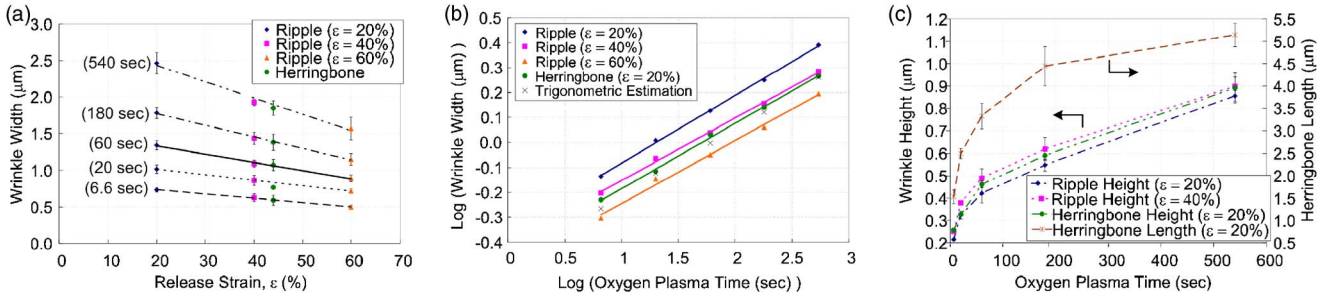

FIG. 3. (Color online) Characterization of ripple and herringbone structures formed under different conditions. The strains listed in the legends indicate the prestrain amount (ε) before oxygen plasma treatment. The straight lines in (a) and (b) are linear fitting of the data. (a) Final ripple width vs release strain at different oxygen plasma times and stretch amounts. (b) Log-log plot of final ripple and herringbone widths vs oxygen plasma time. (c) Final ripple and herringbone amplitude (left Y axis) and herringbone length (right Y axis) vs oxygen plasma time.

$$\varepsilon_c = \frac{1}{4}\left(\frac{3E_s(1-\nu_t^2)}{E_t(1-\nu_s^2)}\right)^{2/3}$$

is the critical strain for buckling, and E, ν, λ_0, A_0, t, and ε_{pre} are Young's modulus, Poisson ratio, ripple wavelength (or width), amplitude, thickness, and prestrain of the sample, respectively. The subscript s and t denote substrate and thin layer, respectively. Our attempt to calculate the ripple characteristics using Eq. (1) was found unsatisfactory. In addition, Eq. (1) assumes stress-free bilayer structure, whereas our system deals with large deformation (up to 60% prestrain) thus, the shear force needs to be taken into account[10] but was ignored in Eq. (1).

Nevertheless, Eq. (1) does provide a useful guidance of the pattern characteristics in our system. Figure 3(a) summarizes the ripple wavelength (or width) versus release strain at different oxygen plasma times and prestrain levels. The ripple wavelength increases as the oxygen plasma time increases, thus, increasing either Young's modulus or thickness that makes the oxide layer harder to bend. The ripple wavelength decreases as the prestrain level increases, which confirms that a denser packing of wrinkles is needed to accommodate a larger strain. It suggests that we should expect a linear relationship between $\log \lambda_0$ and $\log E_t$ or $\log t$ with a slope of 1/3 or 1, respectively, for a small prestrain level ($<10\%$), where the initial buckling takes place. Interestingly, in a log-log plot Fig. 3(a), we found that the *final* wrinkle width λ at a much larger prestain level (20%–60%) was linearly proportional to the oxygen plasma time with a slope of 0.25–0.27 [Fig. 3(b)]. The positive slope with a value smaller than 1/3 suggests that the relation between E_t or t versus oxygen plasma time should be monotonic increase but with power less than one.

Experimentally, we do observe a simple trigonometric relationship between the ripple width and the final highly ordered zigzag-based herringbone width [Fig. 3(b)]. In addition, if we neglect the directional effect of strain but consider the reduction of total area during stretch release process, we should expect that the herringbone with the 20% prestrain in both planar directions would be "equivalent" to 44% prestrain in only one direction, which we did see a surprisingly good match, Fig. 3(a).

The other two characteristics of herringbone patterns are length L and characteristic angle α. Herringbone length [Fig. 3(c)] presented a similar monotonic increase trend versus oxygen plasma time as that of the ripple patterns. Unlike the sinusoidal wavy ripple pattern, most of final herringbones formed in our experiment showed a sharp turning angle of $\sim 80° - 100°$ regardless of oxygen plasma time.

In summary, using mechanical force induced internal buckling on PDMS bilayers, we show maneuver from flat film to 1D ripple, ripple with bifurcation, ripple/herringbone mixture, and to highly ordered 2D herringbone structures by independently control the amount (20%–60%) and timing of large strains on both planar directions. We discover that when equal but sequential strains are applied to the oxide-on-PDMS layer, followed by sequential release in the reverse order, highly ordered zigzag wrinkles can be formed, which is in sharp contrast with random herringbone structures generated by equally and simultaneously applied strain induced by heat or mechanical force. To elucidate the mechanisms of pattern formation under large strain levels and the transition between patterns, we study the variables such as widths, heights, and other characteristics of wrinkles between ripple and herringbone structures. We believe that our study suggests a robust method to vary surface topography reversibly in real time, which may open a gateway to dynamically tune surface properties (wetting, adhesion, and friction).

The authors gratefully thank Daniel E. Koditschek at University of Pennsylvania and Anand Jagota at Lehigh University for helpful discussion. This work was partially supported by National Science Foundation CAREER Award No. DMR-0548070. One of the authors (S.Y.) would also thank the 3M Non-tenured Faculty Grant.

[1] J. Genzer and J. Groenewold, Soft Matter **2**, 310 (2006).
[2] D. Y. Khang, H. Q. Jiang, Y. Huang, and J. A. Rogers, Science **311**, 208 (2006).
[3] E. P. Chan and A. J. Crosby, Adv. Mater. (Weinheim, Ger.) **18**, 3238 (2006).
[4] C. M. Stafford, C. Harrison, K. L. Beers, A. Karim, E. J. Amis, M. R. Vanlandingham, H. C. Kim, W. Volksen, R. D. Miller, and E. E. Simonyi, Nat. Mater. **3**, 545 (2004).
[5] N. Bowden, S. Brittain, A. G. Evans, J. W. Hutchinson, and G. M. Whitesides, Nature (London) **393**, 146 (1998).
[6] N. Bowden, W. T. S. Huck, K. E. Paul, and G. M. Whitesides, Appl. Phys. Lett. **75**, 2557 (1999).
[7] Z. Y. Huang, W. Hong, and Z. Suo, J. Mech. Phys. Solids **53**, 2101 (2005).
[8] X. Chen and J. W. Hutchinson, Scr. Mater. **50**, 797 (2004).
[9] D. B. H. Chua, H. T. Ng, and S. F.. Y. Li, Appl. Phys. Lett. **76**, 721 (2000).
[10] Howard. G. Allen, *Analysis and Design of Structural Sandwich Panels*, 1st ed. (Pergamon, New York, 1969).
[11] X. Chen and J. W. Hutchinson, ASME Trans. J. Appl. Mech. **71**, 597 (2004).